HHS Public Access

Author manuscript

J Vasc Interv Radiol. Author manuscript; available in PMC 2021 May 01.

Published in final edited form as:

J Vasc Interv Radiol. 2020 May ; 31(5): 812–819.e1. doi:10.1016/j.jvir.2019.08.031.

Transarterial Chemoembolization in a Woodchuck Model of Hepatocellular Carcinoma

William F. Pritchard, MD, PhD,
Center for Interventional Oncology, Radiology and Imaging Sciences, Clinical Center, National Institutes of Health, 10 Center Drive, Room 3N320B, MSC 1182, Bethesda, Maryland, USA 20892

David L. Woods, MS,
Center for Interventional Oncology, Radiology and Imaging Sciences, Clinical Center, National Institutes of Health, Bethesda, Maryland, USA 20892

Juan A. Esparza-Trujillo, MS,
Center for Interventional Oncology, Radiology and Imaging Sciences, Clinical Center, National Institutes of Health, Bethesda, Maryland, USA 20892

Matthew F. Starost, DVM, PhD,
Division of Veterinary Resources, National Institutes of Health, Bethesda, Maryland, USA 20892

Michal Mauda-Havakuk, MD, PhD,
Center for Interventional Oncology, Radiology and Imaging Sciences, Clinical Center, National Institutes of Health, Bethesda, Maryland, USA 20892

Andrew S. Mikhail, PhD,
Center for Interventional Oncology, Radiology and Imaging Sciences, Clinical Center, National Institutes of Health, Bethesda, Maryland, USA 20892

Ivane Bakhutashvili, MD, PhD,
Center for Interventional Oncology, Radiology and Imaging Sciences, Clinical Center, National Institutes of Health, Bethesda, Maryland, USA 20892

Shelby Leonard,
Center for Interventional Oncology, Radiology and Imaging Sciences, Clinical Center, National Institutes of Health, Bethesda, Maryland, USA 20892

Elizabeth C. Jones, MD, MPH, MBA,
Radiology and Imaging Sciences, Clinical Center, National Institutes of Health, 10 Center Drive, Room 1C352, MSC 1182, Bethesda, Maryland, USA 20892

[*]Corresponding Author. Tel.: +1 240-760-0153, FAX +1 301-496-9933: william.pritchard@nih.gov.

Venkatesh Krishnasamy, MD,
Center for Interventional Oncology, Radiology and Imaging Sciences, Clinical Center, National Institutes of Health, Bethesda, Maryland, USA 20892

John W. Karanian, PhD,
Center for Interventional Oncology, Radiology and Imaging Sciences, Clinical Center, National Institutes of Health, Bethesda, Maryland, USA 20892

Bradford J. Wood, MD
Center for Interventional Oncology, Radiology and Imaging Sciences, Clinical Center, National Institute of Biomedical Imaging and Bioengineering and National Cancer Institute Center for Cancer Research; National Institutes of Health, Bethesda, Maryland, USA 20892

Abstract

Purpose: To assess the feasibility of transarterial chemoembolization with drug eluting embolics (DEE) in a woodchuck model of hepatocellular carcinoma (HCC).

Materials and Methods: Nine woodchucks were studied: 4 normal animals and 5 infected with woodchuck hepatitis virus that had developed HCC. Three animals with HCC underwent multidetector CT (MDCT). A 3F sheath was introduced into the femoral artery and the hepatic arteries were selectively catheterized with 2.0-2.4 F microcatheters. Normal animals underwent diagnostic angiography and bland embolization. Animals with HCC underwent DEE transarterial chemoembolization with 70-150μm radiopaque microspheres loaded with 37.5 mg doxorubicin per ml. Cone-beam CT and MDCT were performed. Following euthanasia, explanted livers underwent microCT, histopathology and fluorescence imaging of doxorubicin.

Results: The tumors were hypervascular and supplied by large caliber tortuous vessels with arteriovenous shunts present in two animals. There was heterogeneous enhancement on MDCT with areas of necrosis. Six tumors were identified. The most common location was the right medial lobe (n=3). The mean tumor volume (± SE) was 30.7 cm^3 (± 12.3 cm^3). DEE chemoembolization of tumors was achieved. Excluding the two animals with arteriovenous shunts, the mean (± SE) volume of DEE injected was 0.49 ± 0.17 ml. Fluorescence imaging showed diffusion of doxorubicin from the DEE into the tumor.

Conclusion: Woodchuck HCC shares imaging appearances and biological characteristics with human HCC. Selective catheterization and DEE chemoembolization may similarly be performed. Woodchucks may be used to model interventional therapies and possibly characterize radiologic-pathologic correlations.

Introduction

In optimizing current transarterial therapies and translating new treatments, including new combination therapies, for human use, preclinical animal models that closely match the characteristics of human hepatocellular carcinoma (HCC) are valuable. Preclinical studies in interventional oncology for treatment of HCC that rely on mouse and rat tumor models are limited by the animals' small size as well as significant differences in biology compared to human HCC tumors [1]. Rabbits with VX2 tumors may be treated with clinical devices but the biology of the tumors is quite different from HCC limiting extrapolation of results to

clinical applications. Evaluation of transarterial therapies may benefit from a model that more closely encompasses the natural course of the underlying liver disease, with similar tumor size, vascular supply, and heterogeneity, as human liver tumors [2].

Eastern woodchucks (Marmota monax) infected with woodchuck hepatitis virus (WHV) have been used to assess the safety and efficacy of antiviral compounds for hepatitis B virus infection [3–5]. Chronic WHV infection also results in spontaneous development of HCC, making this a useful model to evaluate therapies intended to treat hepatitis-induced tumors in humans [6–10]. Woodchucks also possess hepatic arterial anatomy that can be accessed via the femoral artery and selectively catheterized using clinical microcatheters [11, 12]. Imaging of tumors in woodchucks has been reported in development of imaging agents, assessment of therapeutic interventions or characterization of the tumors using ultrasound [10, 13–15], magnetic resonance imaging [16, 17], and positron emission tomography [18–21]. However, there is limited evaluation of the utility of the woodchuck tumor model for image-guided transcatheter interventional procedures. Needle based optical sensors have been used to delineate the boundary between HCC and normal liver while radiofrequency ablation has been studied with one-week follow-up [7, 9]. Wilkins, et al., showed the feasibility of hepatic lobar arterial catheterization and embolization in normal animals [12]. The purpose of the study was to assess the feasibility of transarterial chemoembolization with drug eluting embolics (DEE) in a woodchuck model of HCC.

Materials and Methods

Animal procedures

The study was conducted under an animal use protocol approved by the Institutional Animal Care and Use Committee in compliance with the U.S. Animal Welfare Regulations. Nine woodchucks (2.5-4.9 kg) were acquired (Northeastern Wildlife, Harrison, Idaho, USA): N=4 tumor negative (mean weight 3.13 kg; 2 females:2 males) and N=5 tumor positive (mean weight 3.88 kg; 3 females:2 males). Tumor positive woodchucks had been infected with WHV within their first week of life and confirmed by the vendor as tumor positive based on serum γ-glutamyl transpeptidase (GGT) level greater than 50 IU/L [22]. Animals were individually housed with 12-hour light:dark cycling and ad libitum access to food and water. Enrichment was provided.

Animals were sedated using 5% isoflurane delivered via an induction chamber followed by a mixture of pre-anesthetics (28.6 mg/kg ketamine HCl and 5 mg/kg xylazine IM) and then maintained on 1-5% isoflurane and 100% oxygen (2 L/min) delivered via rabbit mask for the duration of the procedure. Under anesthesia the animal was shaved and prepared using clean technique. For three tumor positive animals, a jugular cutdown was performed and an 18G angiocatheter was inserted and secured to the skin with suture for pre-procedural MDCT imaging (Philips Brilliance MX8000 IDT 16-section Detector CT; Philips, Andover, MA, USA). Following non-contrast MDCT of the chest and liver, multiphase imaging of the liver was performed with power injection (Medrad Stellant CT Injection System, Bayer Healthcare) via the jugular vein of 3.0 ml of iopamidol (Isovue-370, Bracco Diagnostics) followed by 3.0 ml 0.9% saline all at 0.2 ml/sec. Using CT bolus tracking as measured in the distal thoracic aorta to initiate the scan, multiphasic imaging was acquired in the early

arterial (4 sec delay), late arterial (23 sec delay), portal venous (43 sec delay), and late parenchymal (63 sec) phases. Scans were obtained at 120 kVp and a tube current of 225 mA with a 180 cm field of view and image reconstruction of 0.8 mm sections at 0.4 mm intervals.

Angiography and Embolization

Angiography and transarterial embolization were performed by a radiologist with 35 years of experience. For all animals, a femoral cutdown was performed and a 3 F introducer sheath (Cook, Bloomington, IN, USA) inserted. Hepatic artery catheterization was performed over a 0.014 wire (Runthrough NS Hypercoat, Terumo Medical Corporation, Somerset, NJ; Transcend, Boston Scientific, Marlborough, MA) with a 2.0 F microcatheter (Excelsior 1018, Stryker Neurovascular, Fremont, CA, USA) or 2.4 F microcatheter (Progreat Microcatheter System, Terumo; Merit Maestro Microcatheter, Merit Medical Systems, Inc, South Jordan, UT). Positioning of the catheter was conducted under fluoroscopic guidance (Allura Xper FD20 X-ray System, Philips). Digital subtraction angiography was performed with hand-injection of a 50:50 mixture of 0.9% saline:iopamidol contrast (Isovue-370). For the tumor-bearing animals, selective catheterization was performed under fluoroscopic guidance using angiographic road mapping to minimize contrast administration. Nitroglycerine, 50-100 μg (American Regent, Inc., Shirley, NY) was administered through the microcatheter to minimize vascular spasm.

For the normal animals, 70-150 μm radiopaque microspheres (LC Bead LUMI, Biocompatibles BTG, Farnham, UK) mixed at a dilution of 1 part microspheres to 9 parts 100% iohexol (Omnipaque 350) were injected slowly under fluoroscopy while rotating the syringe for uniform suspension until blood flow stasis was achieved. Stasis was defined by complete occlusion of the target vessels with minor reflux. For tumor-bearing animals, the radiopaque microspheres were loaded with 37.5 μg of doxorubicin per ml. The DEE were then suspended in iohexol contrast media and delivered in the same manner as the bland radiopaque microspheres. In one animal with a large arteriovenous shunt, embolization was halted due to passage of the DEE into the lungs as identified on fluoroscopy.

Post-embolization imaging and analyses

Post-embolization CBCT was performed and woodchucks were euthanized by administration of a combination of pentobarbital sodium 390mg/ml and phenytoin sodium 50mg/ml (Euthasol 1 ml/10 lb; Virbac Animal Health, Fort Worth, TX, USA). Post mortem explant specimen radiography was performed. Hepatic and tumor tissue were collected and frozen before being processed for sectioning and staining with hematoxylin and eosin (H&E) for histopathology. For fluorescence imaging, slides were counterstained with TO-PRO-3 (Invitrogen, Carlsbad, CA) to identify cell nuclei. Two independent channels were captured: Cy5 for nuclei (blue) and a custom filter cube (excitation, 480/40 nm; emission, 600/60 nm) corresponding to excitation and emission spectra (red) of doxorubicin using an epifluorescence microscope (Axio Imager.M1; Zeiss, Thornwood, NY) equipped with a 10X objective (pixel size, 0.64 μm), monochrome charge-coupled device camera, and Zen imaging software (Zeiss).

Results

Pre-procedural MDCT Imaging

Pre-procedural multiphasic contrast-enhanced MDCT images were obtained from three tumor bearing woodchucks. The tumors were hypervascular with arterial enhancement in the early or late arterial phases. The tumors had large caliber tortuous arteries and were heterogeneous in appearance with regions of hyper- and hypo- enhancement, necrotic regions, lipid deposition and a nodule-within-nodule pattern, resembling features of human HCC. Representative CT images of a single woodchuck bearing two tumors show the various enhancement patterns of liver and tumor (Figure 1). Both the larger, pedunculated tumor and the smaller tumor showed early arterial enhancement (Figure 1 B). The latter also showed contrast wash-out in the late arterial and portal venous phases (Figures 1 C). A low attenuation, non-enhancing region within the larger tumor was observed throughout the different phases representing necrosis as confirmed at pathology.

Angiography and Embolization

Four normal woodchucks underwent diagnostic angiography with catheterization of the celiac axis and then the hepatic artery (Figure 2). The nomenclature of the arterial blood supply is based on the arterial and lobar anatomy as described by Bezuidenhout and Evans [23]. Bland embolization of the normal liver to stasis was successful in all four, with the catheter positioned in the left hepatic artery in 3 animals and in the right hepatic artery in 1 animal, data not shown.

For the five tumor bearing woodchucks, angiography revealed that the vessels supplying the tumors were enlarged (Figures 2C, 2D, 3 and 4). Arteriovenous shunting was also observed in the two largest tumors present in the five woodchucks (Figure 3; Figure E1 A and B available online on the article's Supplemental Material page at www.jvir.org). Of the six tumors identified, three were in the right medial lobe with one each in the papillary process, left medial lobe and quadrate lobe. The mean tumor volume (± SE) was 30.7 cm^3 (± 12.3 cm^3) based on MDCT and CBCT.

Transarterial chemoembolization with doxorubicin DEE was performed in all five animals. In three of the animals, the arteries supplying four tumors were selectively catheterized for embolization: the right hepatic artery in two animals and in the third, the quadrate lobe artery and the left lateral lobe artery (Figure 4). In one of the animals that underwent selective embolization via the right hepatic artery, non-selective embolization of smaller tumors was subsequently performed. In the two remaining animals, DEE chemoembolization was performed from the hepatic artery. While DEE delivery to the tumor was achieved in the animal with the large arteriovenous shunt (Figure 3), embolization was halted due to non-target embolization of the lungs as noted on fluoroscopy. Excluding the two animals with arteriovenous shunts, the mean (± SE) volume of DEE injected was 0.49 ± 0.17 ml. Fluoroscopic imaging, MDCT and CBCT without additional contrast were performed at least 45 minutes after embolization to allow washout of liquid contrast [24], confirming localization of DEE in tumors (Figure 5 A–C). For those animals that underwent selective catheterization and DEE chemoembolization, excised tumors were scanned using

microCT providing greater conspicuity of DEE in distal arteries (Figure 5 D). Nontarget embolization was identified in 4 of the five animals: two with arteriovenous shunts had microspheres in the lungs, one had microspheres identified in the distribution of the gastroduodenal and splenic arteries at pathology and one had microspheres in the distribution of the gastroesophageal artery on post procedural MDCT.

Tumor pathology

Hepatic tumors of variable size and morphology were observed at gross pathologic examination. Large tumors tended to be exophytic or pedunculated while smaller tumors were generally contained within the parenchyma. All tumors were confirmed to be HCC upon histopathologic evaluation by a board-certified veterinary pathologist. Representative histopathology using H&E stained tissue demonstrated variable sized HCC with occasional fibrosis and compression of surrounding parenchyma. In the liver surrounding the tumor, diffuse mild to moderate biliary hyperplasia including notable lymphohistiocytic infiltration of portal tracts as well as patchy areas of hepatic lipidosis were observed. (Fig E2 A and B available online on the article's Supplemental Material page at www.jvir.org)

Doxorubicin drug-eluting embolic histology

Radiopaque DEE (70-150 μm) were visible inside treated intra-tumoral arteries (Figure 6A). Fluorescence microscopy of tumor sections embolized with doxorubicin DEE demonstrated the elution of doxorubicin into surrounding tissue 45 min post-embolization (Figure 6B). A gradient of fluorescence is visible indicating decreasing doxorubicin concentration with increasing distance from the DEE.

Discussion

Transcatheter therapies such as DEE transarterial chemoembolization remain both a standard therapy for HCC as well as a proposed clinical methodology for antigen presentation when combined with immunotherapies for human HCC [25]. The limited animal tumor models suitable for preclinical evaluation and development of novel transarterial interventions hinders the translation of new therapies for treatment of human HCC where transcatheter therapies may play a role. This study demonstrates the feasibility of using a woodchuck HCC tumor model for evaluating transarterial chemoembolization using radiopaque doxorubicin DEE. Imaging and histologic characterization of WHV-induced tumors revealed heterogeneous tumors of varying size, vascular supply, and position within the liver, similar to human HCC. Selective embolization of HCC tumors was achieved using catheter-based procedures and interventional devices marketed for human use.

In a study by Tennant et al, woodchucks chronically infected with WHV at birth developed HCC as early as 9 months with 25% surviving to between 36 and 56 months of age. WHV resembles human hepatitis B virus genetically and biologically. The current work adds imaging phenotypes to this list of similarities with heterogeneous genetic and imaging features across a tumor. Tumorigenesis occurs in the absence of histological cirrhosis [26] which facilitates recognition of a gradual transition spectrum from normal parenchyma to neoplastic nodules to HCC. Woodchucks generally present with multiple tumors of different

sizes that potentially represent different stages of de-differentiation along the WHV carcinogenesis axis [22, 27]. Such a transition may provide an opportunity to evaluate interventions at different stages of HCC development or to better understand this transition. The complex interplay of intra-tumoral and inter-tumoral genetic heterogeneity with the wide variety of imaging phenotypes and histologies at a given time point in their disease development is a defining feature of woodchuck HCC, but needs further characterization.

Arterial embolization of the liver in normal woodchucks has been reported in a small study that showed the potential for catheterization of hepatic lobar arteries and transarterial embolization [12]. The present study demonstrated the feasibility of intra-arterial, selective delivery of radiopaque DEE to hepatic tumors in woodchucks and identified some of the challenges in this naturally occurring disease model, e.g. large arteriovenous shunts. The tumors were hypervascular with arterial blood supply by large caliber, tortuous vessels. Selective catheterization of tumor vasculature resulted in targeted DEE deposition and drug localization. The ability to selectively catheterize tumors may permit the investigation of different embolic agents or drugs within the same animal or even the same tumor, leaving untreated tissue as a control while minimizing embolization of normal liver for survival studies.

Understanding the arterial anatomy of the woodchuck is essential to safe performance of embolization for survival interventions. The left hepatic artery commonly supplies the majority of the woodchuck liver parenchyma with anatomic variations in the branching and hepatic blood supply patterns. It gives rise to the gastroesophageal artery that supplies the abdominal esophagus and cardia of the stomach which should be considered in planning an intervention to avoid non-target embolization (Figures 2A and 2B). The gastroduodenal artery arises from the hepatic artery and should be avoided as well [23]. Arteriovenous intratumoral shunts were observed in two woodchucks.

The radiopacity of the microspheres provides a means for directly monitoring spatial distribution of DEE during and after treatment. It has been shown that the attenuation of radiopaque DEE on CT can be used to predict the dose of drug delivered in embolized tissues [28]. In this study, radiopaque DEE were highly conspicuous on MDCT and appeared densely packed in target blood vessels. Moreover, high resolution imaging of explanted livers on microCT provided visualization of DEE in distal vasculature, as previously described in swine [29]. Successful targeted drug delivery was confirmed upon microscopic examination of doxorubicin fluorescence in tissue sections, demonstrating drug elution from the DEE into surrounding tumor tissue. Combining visualization of radiopaque DEE with quantitative measure of drug pharmacokinetics and pharmacodynamics in a predictive animal model of HCC may advance development of drug dosimetry and new combination therapies.

An ideal animal HCC tumor model should resemble human tumors in etiology, underlying liver disease, microenvironment, heterogeneity, vascularity and genomic alterations. An autochthonous rat model was recently introduced for investigation of interventional oncology paradigms in which tumors are induced by administration of the toxin diethylnitrosamine. While the model offers the advantage of recapitulating much of the

biology of human HCC, performing embolizations in this scaled down model is time consuming and associated with a steep learning curve [5, 30]. Among mouse models of HCC, those induced by diethylnitrosamine show the least genetic similarity to human HCC [1].

The rabbit VX2 tumor model is an orthotopic model commonly used as an HCC model for interventional procedures to evaluate local thermal ablation and embolization [31–33]. The model uses donor rabbits for propagation of tumor cells prior to orthotopic allografting into the liver of recipient rabbits via percutaneous injection or laparotomy. However, VX2 tumors differ dramatically in cellular biology from human HCC and are often subject to large amounts of spontaneous central necrosis which confounds evaluation of treatment effects, especially with focal ablation or embolization techniques where this necrosis may prevent realistic local or regional therapy [2, 34]. In addition, tumor growth can be inconsistent including short survival periods following inoculation, limiting suitability of the model for long term efficacy studies [34]. The spontaneous and slower growth rate of woodchuck tumors relative to VX2 tumors may facilitate tumoral arterial hypertrophy, encompass an immune response that better recapitulates the human HCC microenvironment, and may enable longitudinal efficacy studies.

The woodchuck model has limitations. The model can be expensive and requires specialized husbandry and veterinary management. Anesthesia of woodchucks is complicated by their hibernation cycle resulting in seasonal changes in respiration, metabolism and anesthesia management that makes them vulnerable to adverse events. While the slow rate of tumor growth permits long term follow-up after intervention, the timeline for tumor development after establishing chronic WHV infection creates longer study timelines for scientific investigations, placing greater pressure on resources. Several aspects of the model remain to be characterized including woodchuck genomic profile and antigenic markers. In this regard, the availability of experimental tools and molecular probes is limited.

In summary, this study demonstrated that woodchucks with WHV develop HCC with imaging appearance and biological characteristics similar to those of human HCC which facilitate selective arterial catheterization and chemoembolization. These findings support the use of this model for translational research in interventional oncology and the development of image-guided therapy algorithms. The woodchuck model and radiology-pathology correlations may facilitate development and assessment of novel therapies in human HCC that include local and regional interventions such as radiopaque DEE-transarterial chemoembolization.

Supplementary Material

Refer to Web version on PubMed Central for supplementary material.

Acknowledgments:

The authors would like to thank Lisa Portnoy, DVM, Joanne Smith, DVM, and the staff of the Division of Veterinary Resources, National Institutes of Health for providing their expertise and animal care for the study. We also thank Bud C. Tennant, DVM, and Patrick W. Concannon, PhD of Cornell University; Paul J. Cote, PhD,

Stephan Menne, PhD, and Robin D. Tucker, DVM of Georgetown University; and, James Whipple and Jamie L. Hass DVM PhD of Northeastern Wildlife for sharing their expertise with regards to woodchucks.

Financial Support Statement and Conflict of Interest Statement:

This work was supported by the Center for Interventional Oncology in the Intramural Research Program of the National Institutes of Health (NIH) by intramural NIH Grants NIH Z01 1ZID BC011242 and CL040015. Dr. Mauda-Havakuk is supported by the Intramural Program of National Institute for Biomedical Imaging and Bioengineering. The NIH and Biocompatibles BTG UK have a Cooperative Research and Development Agreement which provided funding for the conduct of the study. Biocompatibles BTG UK had no control over the conduct of the study, the inclusion of any data, data analysis and interpretation, manuscript preparation and decisions on submission for publication. NIH may hold intellectual property in the field. NIH has a Materials Transfer Agreement with Northeastern Wildlife.

References

[1]. Dow M, Pyke RM, Tsui BY, et al. Integrative genomic analysis of mouse and human hepatocellular carcinoma. Proc Natl Acad Sci U S A 2018; 115:E9879–E88. [PubMed: 30287485]

[2]. Obeid M, Khabbaz R, Garcia K, Schachtschneider K, Gaba R. Translational Animal Models for Liver Cancer. American Journal of Interventional Radiology 2018; 2:1–8.

[3]. Menne S, Cote PJ. The woodchuck as an animal model for pathogenesis and therapy of chronic hepatitis B virus infection. World Journal of Gastroenterology 2007; 13:104–24. [PubMed: 17206759]

[4]. Roggendorf M, Kosinska AD, Liu J, Lu M. The Woodchuck, a Nonprimate Model for Immunopathogenesis and Therapeutic Immunomodulation in Chronic Hepatitis B Virus Infection. Cold Spring Harb Perspect Med 2015; 5.

[5]. Balsitis S, Gali V, Mason PJ, et al. Safety and efficacy of anti-PD-L1 therapy in the woodchuck model of HBV infection. PLoS One 2018; 13:e0190058. [PubMed: 29444087]

[6]. Huang KW, Wu HL, Lin HL, et al. Combining antiangiogenic therapy with immunotherapy exerts better therapeutical effects on large tumors in a woodchuck hepatoma model. Proc Natl Acad Sci U S A 2010; 107:14769–74. [PubMed: 20679198]

[7]. Burke CT, Cullen JM, State A, et al. Development of an animal model for radiofrequency ablation of primary, virally induced hepatocellular carcinoma in the woodchuck. J Vasc Interv Radiol 2011; 22:1613–8 e1. [PubMed: 21959057]

[8]. Buendia MA, Neuveut C. Hepatocellular carcinoma. Cold Spring Harb Perspect Med 2015; 5:a021444. [PubMed: 25646384]

[9]. Nachabe R, Hendriks BHW, Schierling R, et al. Real-Time In Vivo Characterization of Primary Liver Tumors With Diffuse Optical Spectroscopy During Percutaneous Needle Interventions Feasibility Study in Woodchucks. Invest Radiol 2015; 50:443–8. [PubMed: 25783227]

[10]. Fairman J, Liu KH, Menne S. Prevention of liver tumor formation in woodchucks with established hepatocellular carcinoma by treatment with cationic liposome-DNA complexes. BMC Cancer 2017; 17:172. [PubMed: 28264666]

[11]. Dahmen U, Radtke A, Schroder T, et al. Median liver lobe of woodchuck as a model to study hepatic outflow obstruction: a pilot study. Liver Int 2008; 28:1236–44. [PubMed: 18544125]

[12]. Wilkins LR, Stone JR, Mata J, Hawrylack A, Kubicka E, Brautigan DL. The Use of the Woodchuck as an Animal Model for Evaluation of Transarterial Embolization. J Vasc Interv Radiol 2017; 28:1467–71. [PubMed: 28941521]

[13]. Forsberg F, Goldberg BB, Liu JB, Merton DA, Rawool NM, Shi WT. Tissue-specific US contrast agent for evaluation of hepatic and splenic parenchyma. Radiology 1999; 210:125–32. [PubMed: 9885597]

[14]. Lisi D, Kondili LA, Ramieri MT, et al. Ultrasonography in the study of hepatocellular carcinoma in woodchucks chronically infected with WHV. Lab Anim 2003; 37:233–40. [PubMed: 12869286]

[15]. Rodriguez-Madoz JR, Liu KH, Quetglas JI, et al. Semliki forest virus expressing interleukin-12 induces antiviral and antitumoral responses in woodchucks with chronic viral hepatitis and hepatocellular carcinoma. J Virol 2009; 83:12266–78. [PubMed: 19740992]

[16]. McKenzie EJ, Jackson M, Sun J, Volotovskyy V, Gruwel ML. Monitoring the development of hepatocellular carcinoma in woodchucks using 31P-MRS. MAGMA 2005; 18:201–5. [PubMed: 16133593]

[17]. McKenzie EJ, Jackson M, Turner A, Gregorash L, Harapiak L. Chronic care and monitoring of woodchucks (Marmota monax) during repeated magnetic resonance imaging of the liver. J Am Assoc Lab Anim 2006; 45:26–30.

[18]. Salem N, MacLennan GT, Kuang Y, et al. Quantitative evaluation of 2-deoxy-2[F-18]fluoro-D-glucose-positron emission tomography imaging on the woodchuck model of hepatocellular carcinoma with histological correlation. Mol Imaging Biol 2007; 9:135–43. [PubMed: 17308952]

[19]. Salem N, Kuang Y, Wang F, Maclennan GT, Lee Z. PET imaging of hepatocellular carcinoma with 2-deoxy-2[18F]fluoro-D-glucose, 6-deoxy-6[18F] fluoro-D-glucose, [1-11C]-acetate and [N-methyl-11C]-choline. Q J Nucl Med Mol Imaging 2009; 53:144–56. [PubMed: 19039303]

[20]. Kuang Y, Salem N, Tian H, et al. Imaging lipid synthesis in hepatocellular carcinoma with [methyl-11c]choline: correlation with in vivo metabolic studies. J Nucl Med 2011; 52:98–106. [PubMed: 21149484]

[21]. Kolthammer JA, Corn DJ, Tenley N, et al. PET imaging of hepatocellular carcinoma with 18F-fluoroethylcholine and 11C-choline. Eur J Nucl Med Mol I 2011; 38:1248–56.

[22]. Jacob JR, Sterczer A, Toshkov IA, et al. Integration of woodchuck hepatitis and N-myc rearrangement determine size and histologic grade of hepatic tumors. Hepatology 2004; 39:1008–16. [PubMed: 15057905]

[23]. Bezuidenhout AJ, Evans HE. Anatomy of the woodchuck (Marmota monax). Lawrence, KS: American Society of Mammalogists, 2005.

[24]. Mikhail AS, Pritchard WF, de Ruiter QMB, et al. Contrast clearance following hepatic transarterial embolization with radio-opaque and non-radio-opaque micro beads in swine. Cardiovasc Intervent Radiol 2018; 41:S179.

[25]. Duffy AG, Ulahannan SV, Makorova-Rusher O, et al. Tremelimumab in combination with ablation in patients with advanced hepatocellular carcinoma. J Hepatol 2017; 66:545–51. [PubMed: 27816492]

[26]. Tennant BC, Toshkov IA, Peek SF, et al. Hepatecellular carcinoma in the woodchuck model of hepatitis B virus infection. Gastroenterology 2004; 127:s283–s93. [PubMed: 15508096]

[27]. Popper H, Roth L, Purcell RH, Tennant BC, Gerin JL. Hepatocarcinogenicity of the woodchuck hepatitis virus. Proc Natl Acad Sci U S A 1987; 84:866–70. [PubMed: 3468514]

[28]. Mikhail AS, Pritchard WF, Negussie AH, et al. Mapping Drug Dose Distribution on CT Images Following Transarterial Chemoembolization with Radiopaque Drug-Eluting Beads in a Rabbit Tumor Model. Radiology 2018; 289:396–404. [PubMed: 30106347]

[29]. Thompson JG, van der Sterren W, Bakhutashvili I, et al. Distribution and Detection of Radiopaque Beads after Hepatic Transarterial Embolization in Swine: Cone-Beam CT versus MicroCT. J Vasc Interv Radiol 2018; 29:568–74. [PubMed: 29500000]

[30]. Gade TP, Hunt SJ, Harrison N, et al. Segmental Transarterial Embolization in a Translational Rat Model of Hepatocellular Carcinoma. J Vasc Interv Radiol 2015; 26:1229–37. [PubMed: 25863596]

[31]. Deng G, Zhao DL, Li GC, Yu H, Teng GJ. Combination therapy of transcatheter arterial chemoembolization and arterial administration of antiangiogenesis on VX2 liver tumor. Cardiovasc Intervent Radiol 2011; 34:824–32. [PubMed: 21671151]

[32]. You Y, Wang Z, Ran H, et al. Nanoparticle-enhanced synergistic HIFU ablation and transarterial chemoembolization for efficient cancer therapy. Nanoscale 2016; 8:4324–39. [PubMed: 26837265]

[33]. Gholamrezanezhad A, Mirpour S, Geschwind JF, et al. Evaluation of 70–150-mum doxorubicin-eluting beads for transcatheter arterial chemoembolization in the rabbit liver VX2 tumour model. Eur Radiol 2016; 26:3474–82. [PubMed: 26780638]

[34]. Aravalli RN, Golzarian J, Cressman EN. Animal models of cancer in interventional radiology. Eur Radiol 2009; 19:1049–53. [PubMed: 19137307]

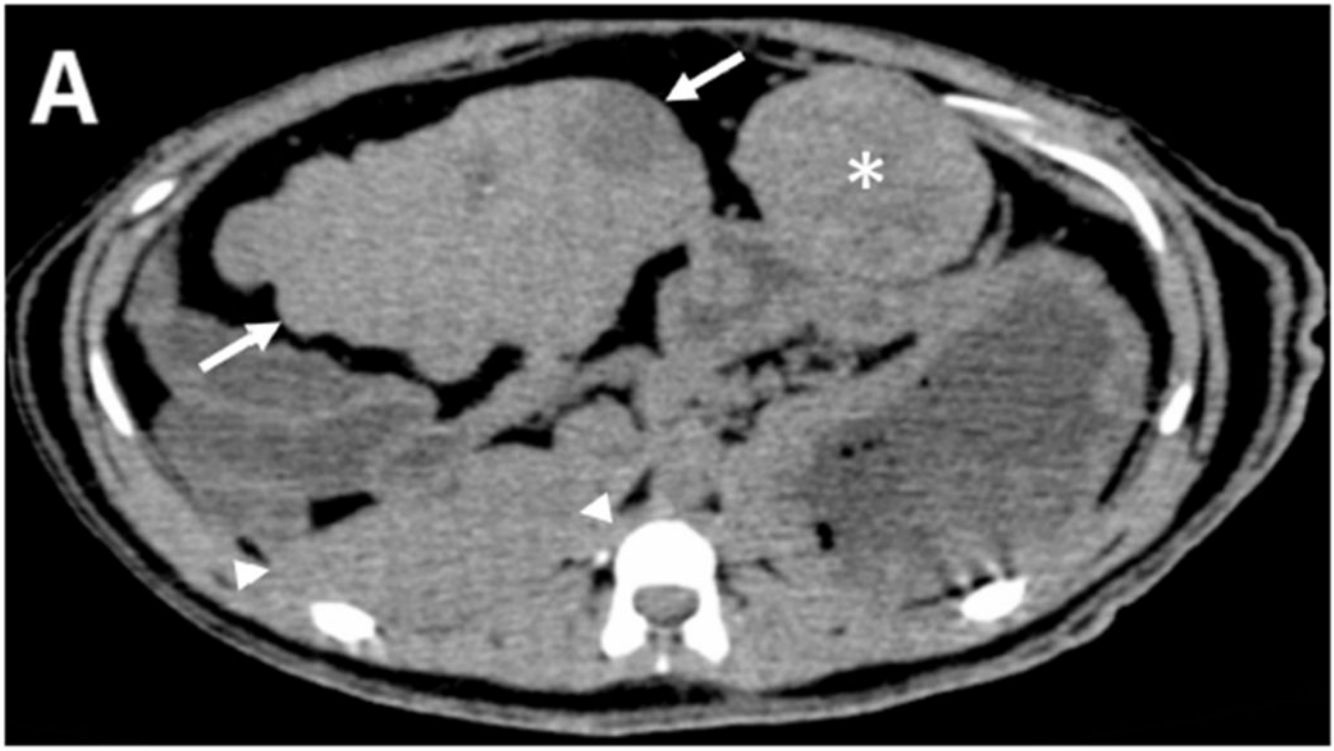

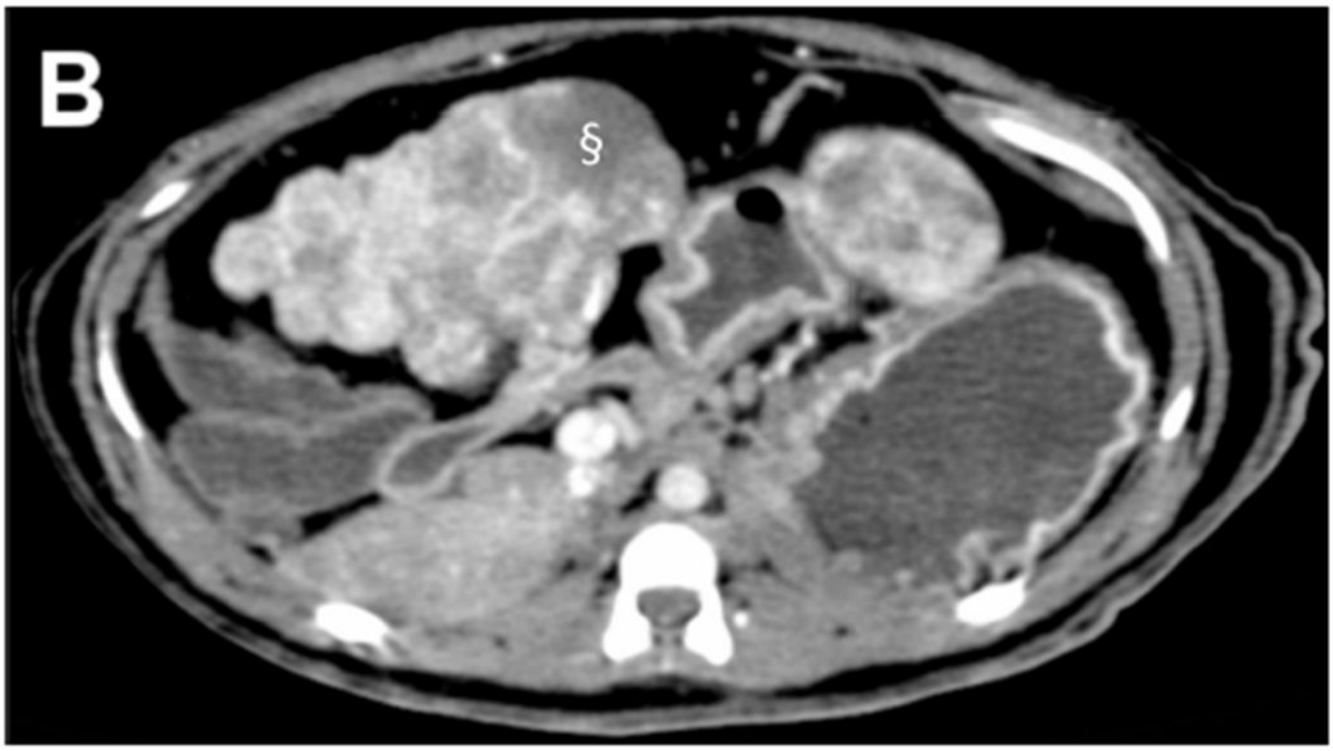

Figure 1.

Pre-procedural contrast enhanced multidetector CT images of two tumors in a woodchuck. (A) Axial image of the upper abdomen without contrast. (B) Early arterial phase image at the same level. (C) Coronal reconstruction of the portal venous phase. The larger, 6 cm pedunculated tumor (arrows) attached to the left medial and quadrate lobes and the smaller 3.2 cm tumor (*) showed early arterial enhancement with washout evident in the smaller tumor. A non-enhancing, low attenuation component of the larger tumor (§) represented an area of necrosis. An area of liver without tumor is shown (arrowheads).

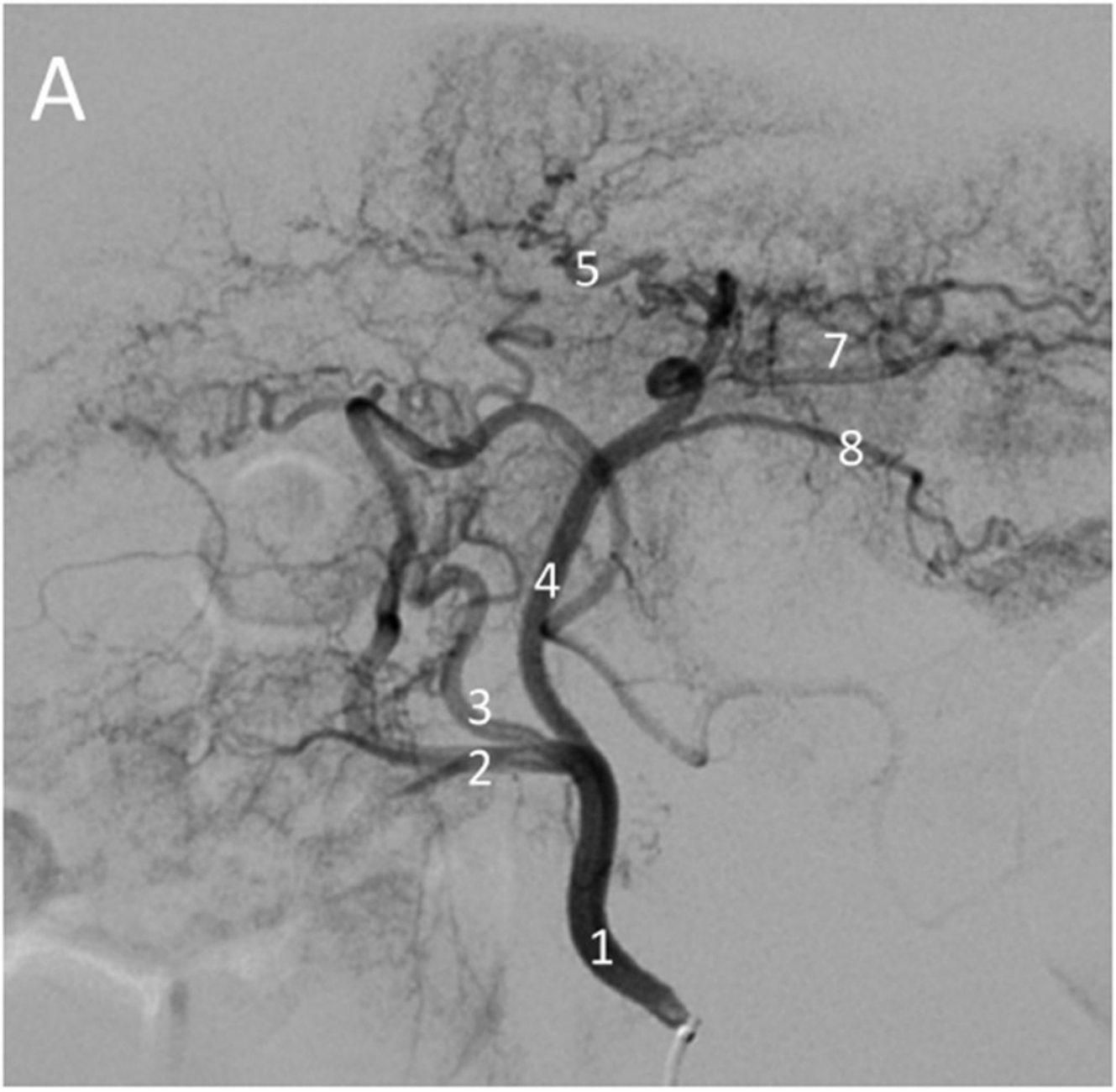

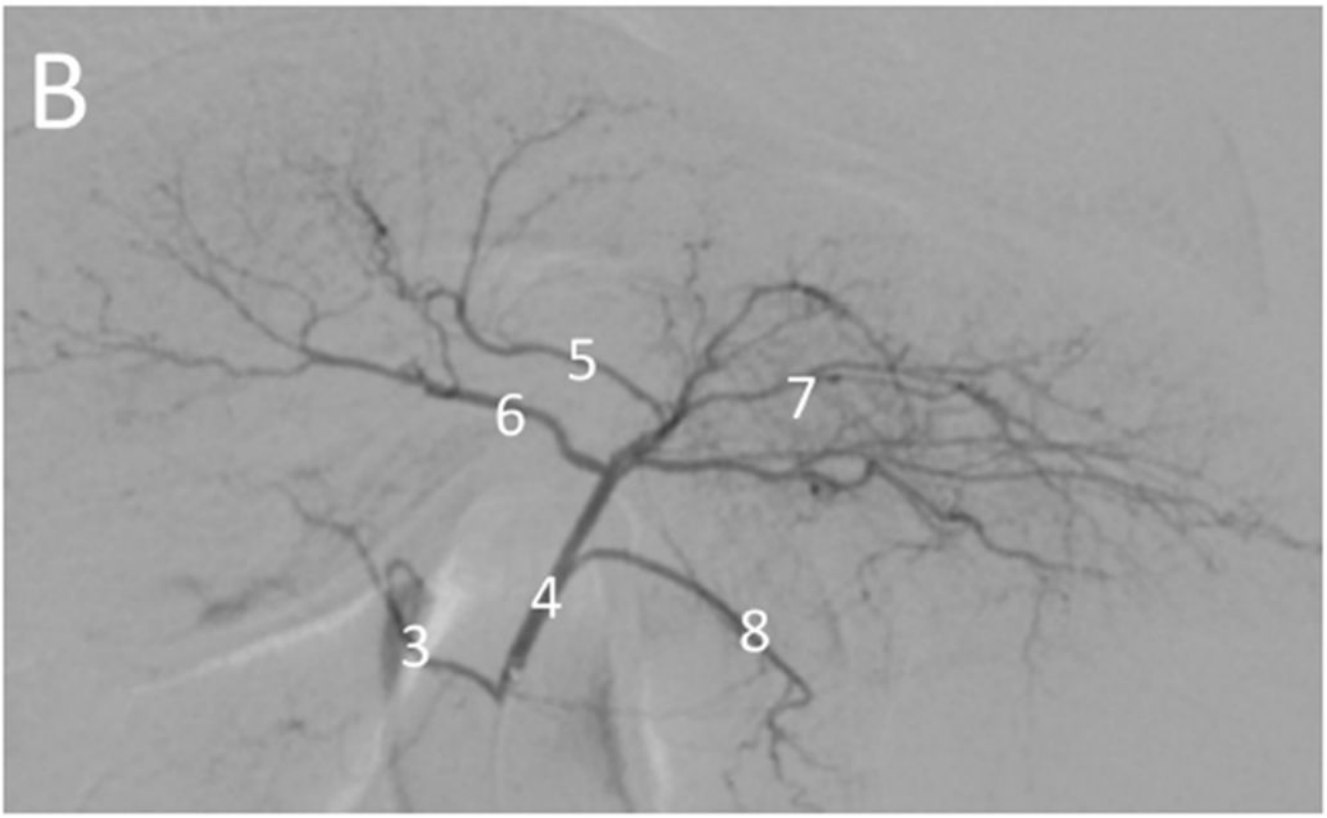

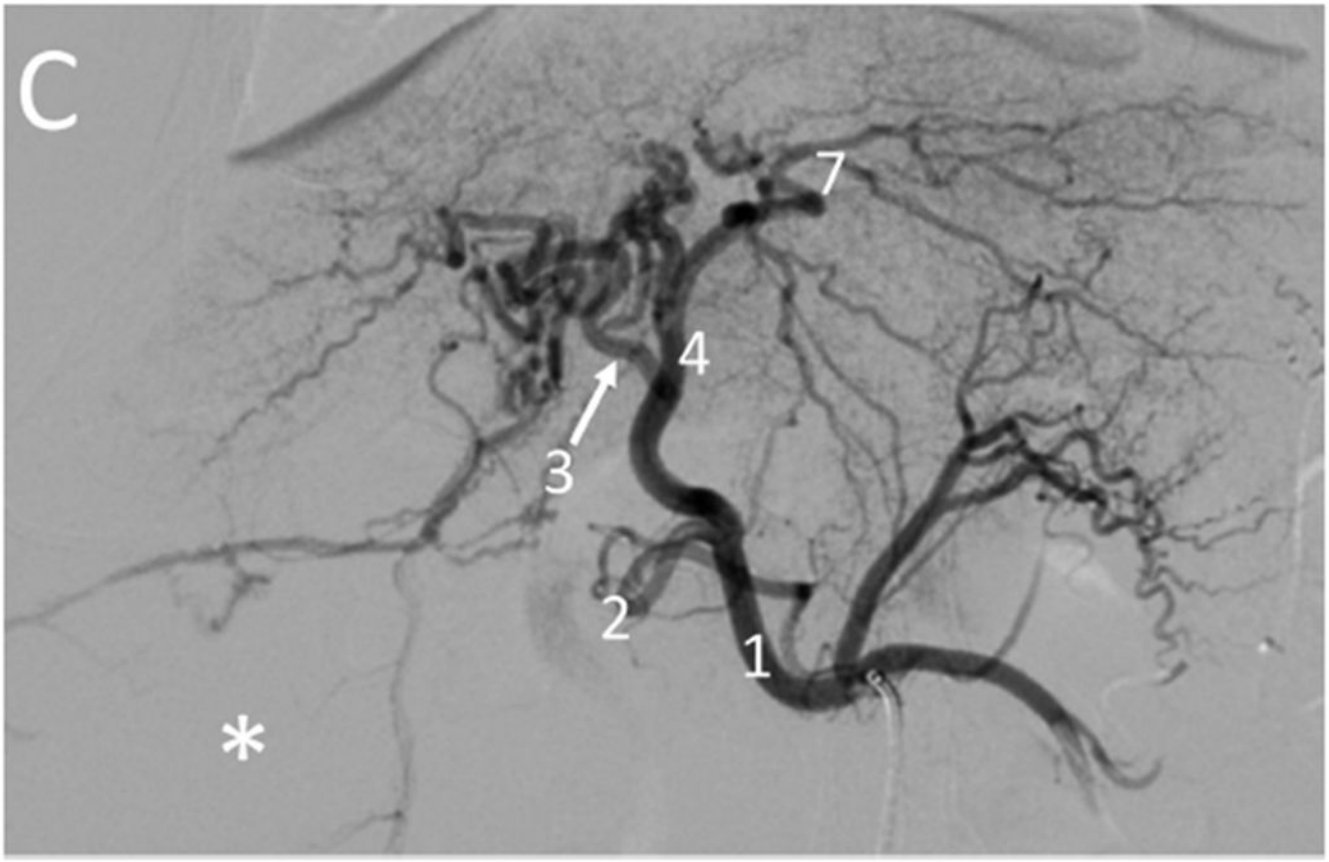

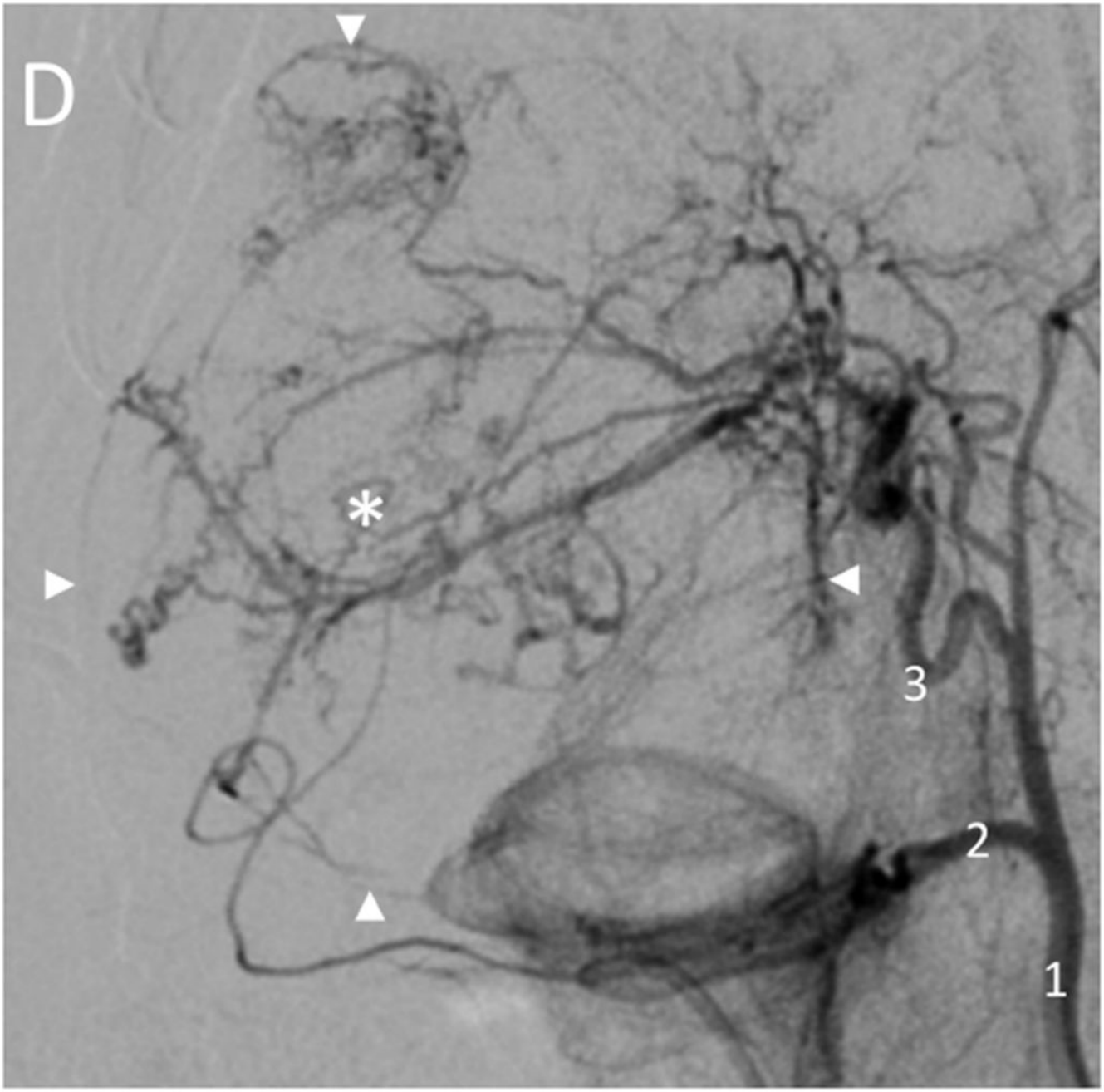

Figure 2.

Hepatic angiography of normal (non-tumor) and tumor-bearing woodchucks. Normal hepatic vasculature (A) following injection of the hepatic artery (1) or (B) injection of the proximal left hepatic artery (4) showing the gastroduodenal artery (2), right hepatic artery (3), left medial lobe artery (5), quadrate lobe artery (6), left lateral lobe arteries (7) and gastroesophageal artery (8). In (A), the gastroduodenal and right hepatic arteries arise from a common branch of the hepatic artery with the right hepatic artery giving rise to the quadrate lobe artery in this anatomic variant. In woodchucks with HCC (C, D), celiac artery injection (C) showing an enlarged right hepatic artery (3, arrow) supplying a large HCC (*). Hepatic

artery injection (D) showing an enlarged right hepatic artery (3) supplying a large HCC (*) delineated by the arrowheads. Abnormal tumor vasculature is evident within the tumor.

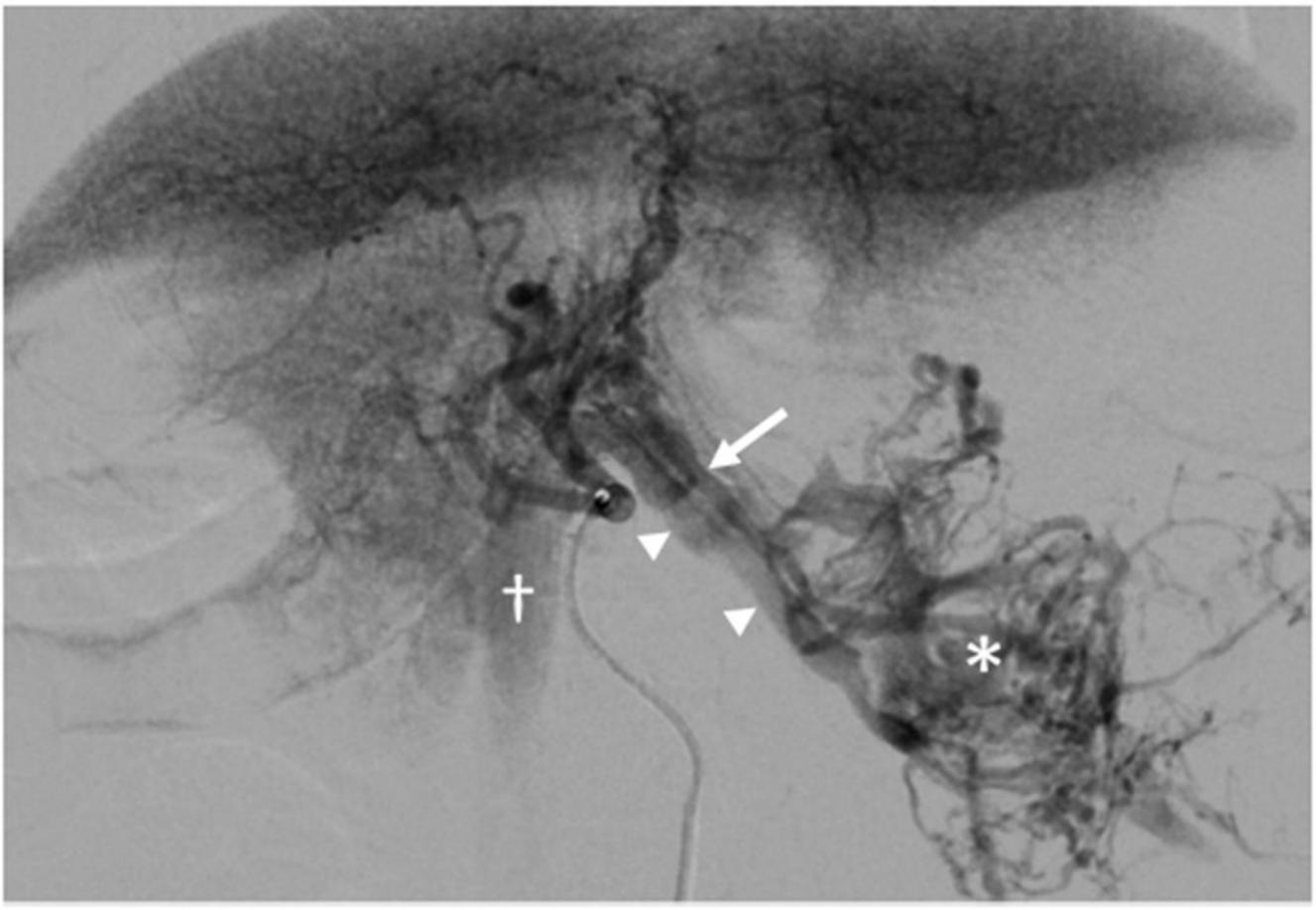

Figure 3.

Large HCC with arteriovenous shunt. The artery (arrow) supplying the HCC (*) is visible with early filling of draining veins (arrowheads) and opacification of the inferior vena cava (†) which contrasts with parenchymal enhancement of normal liver. Arterial and later phase images (Figure E1 A and B) are available online on the article's Supplemental Material page at www.jvir.org.

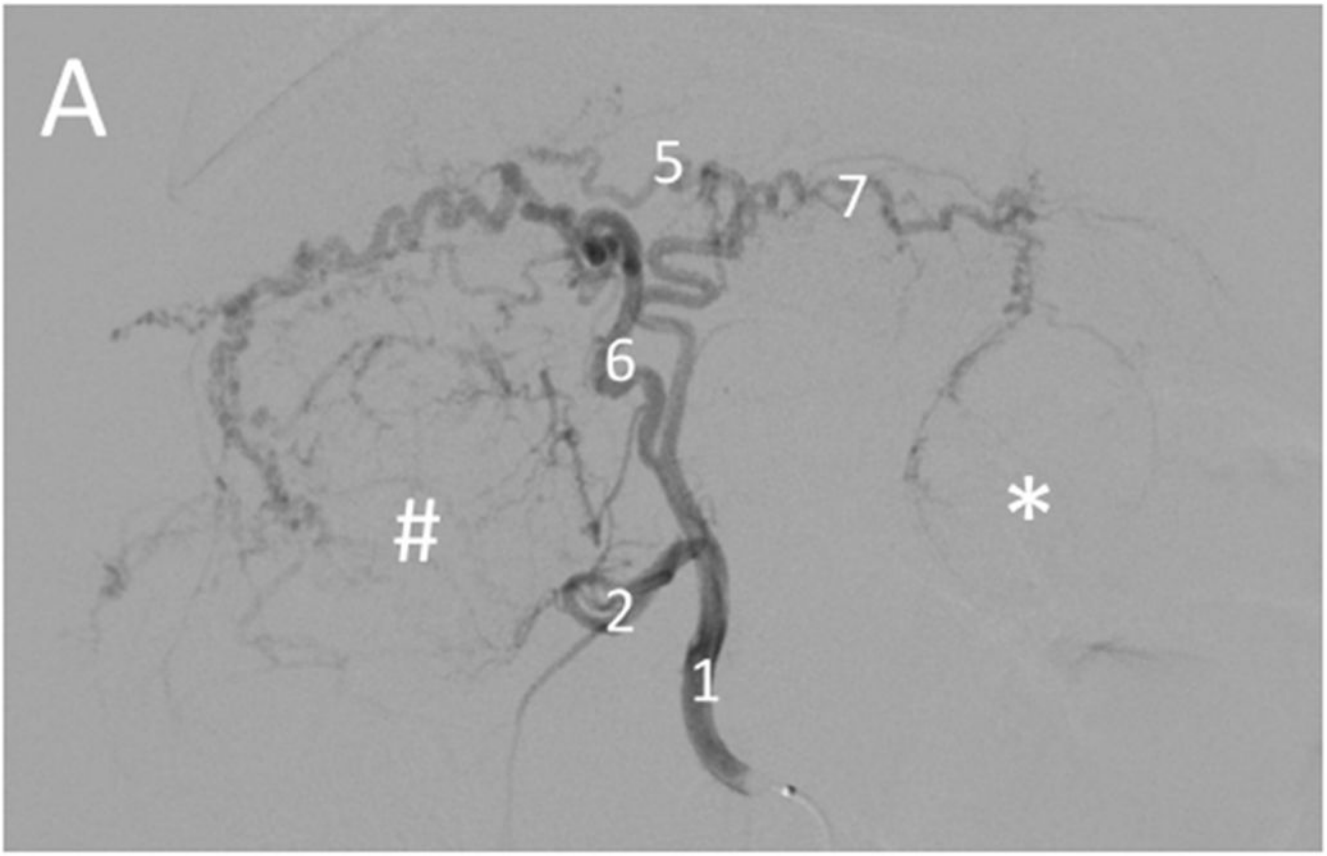

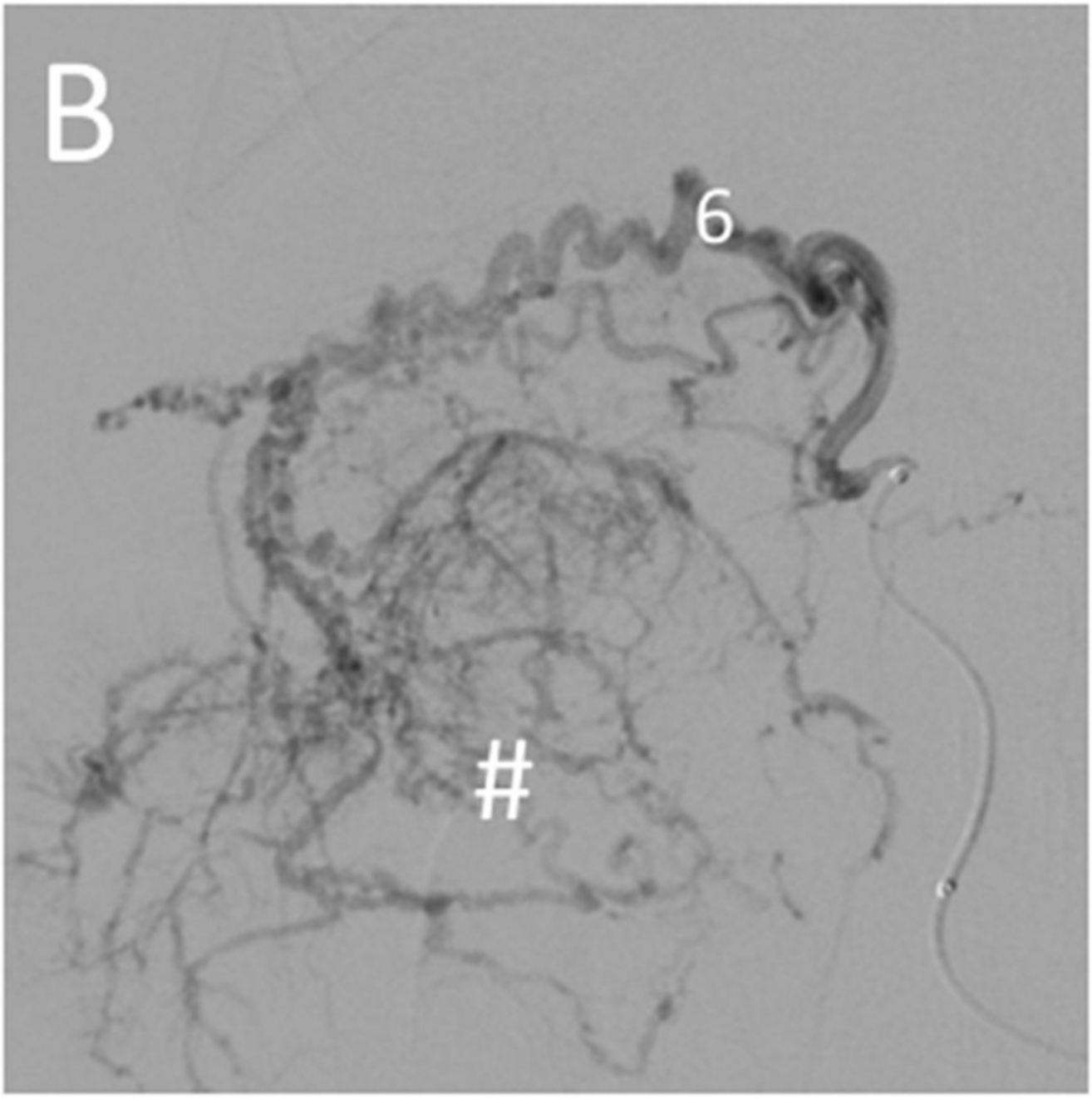

Figure 4.

Selective catheterization of the artery supplying a large tumor. Pre-embolization digital subtraction angiography for the woodchuck shown in Figures 1 and 5. (A) Hepatic artery (1) injection showing the arterial supply of the two tumors: the right tumor (#) by the quadrate lobe artery (6) and the left tumor (*) by the left lateral lobe artery (7). The gastroduodenal artery (2) and left medial lobe artery (5) are also shown. (B) Selective catheterization and angiography of the quadrate lobe artery (6) supplying the tumor on the right (#).

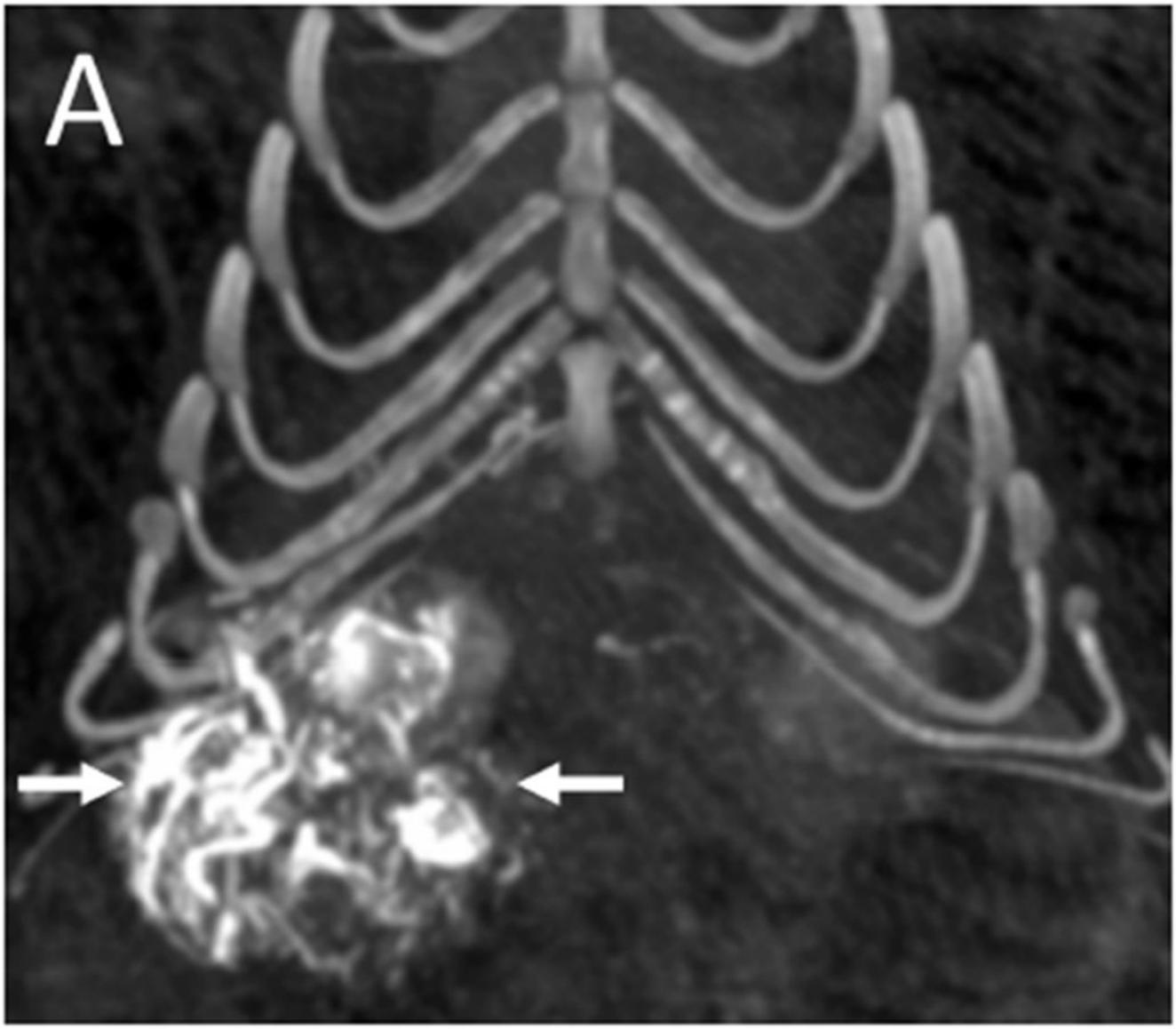

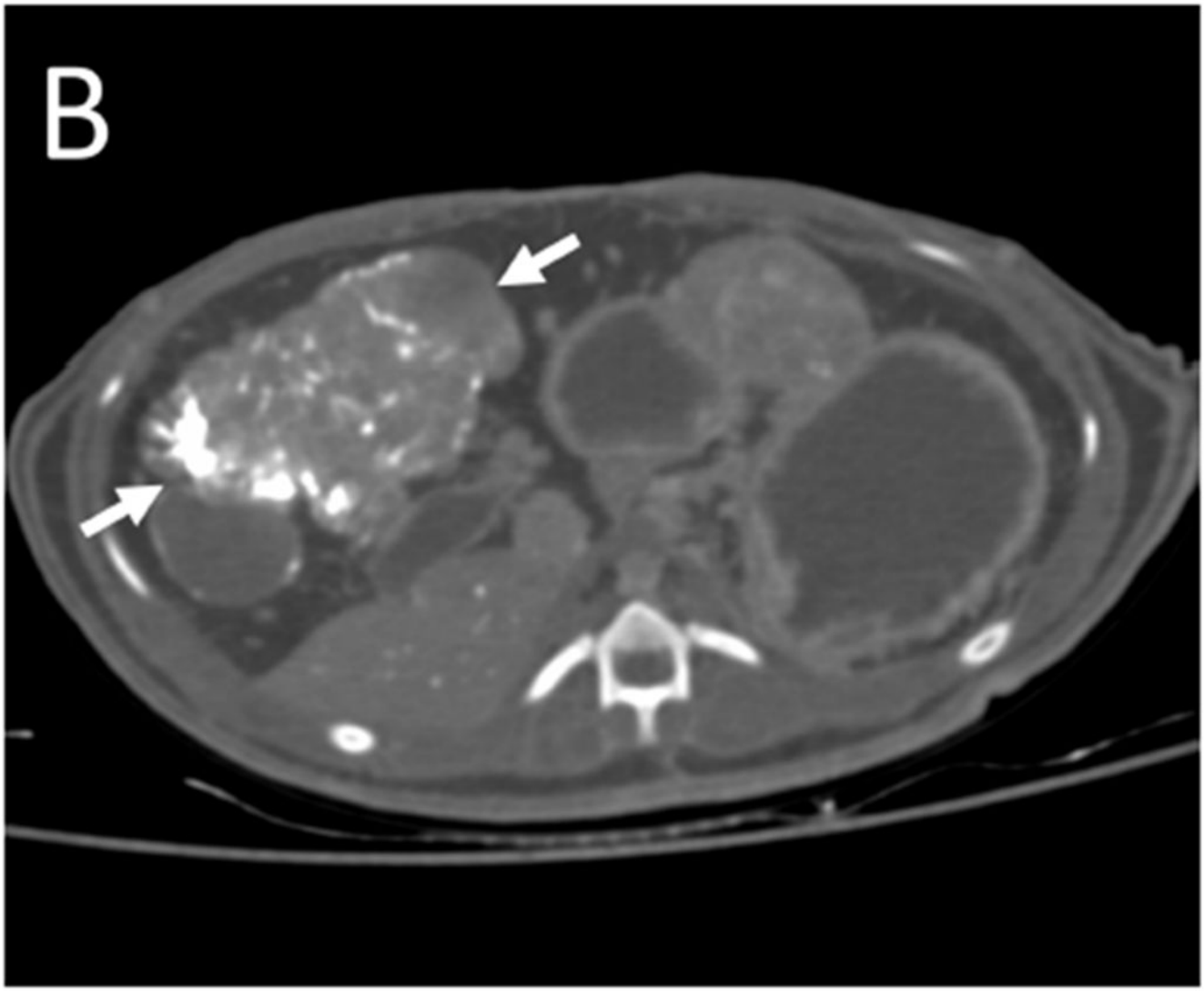

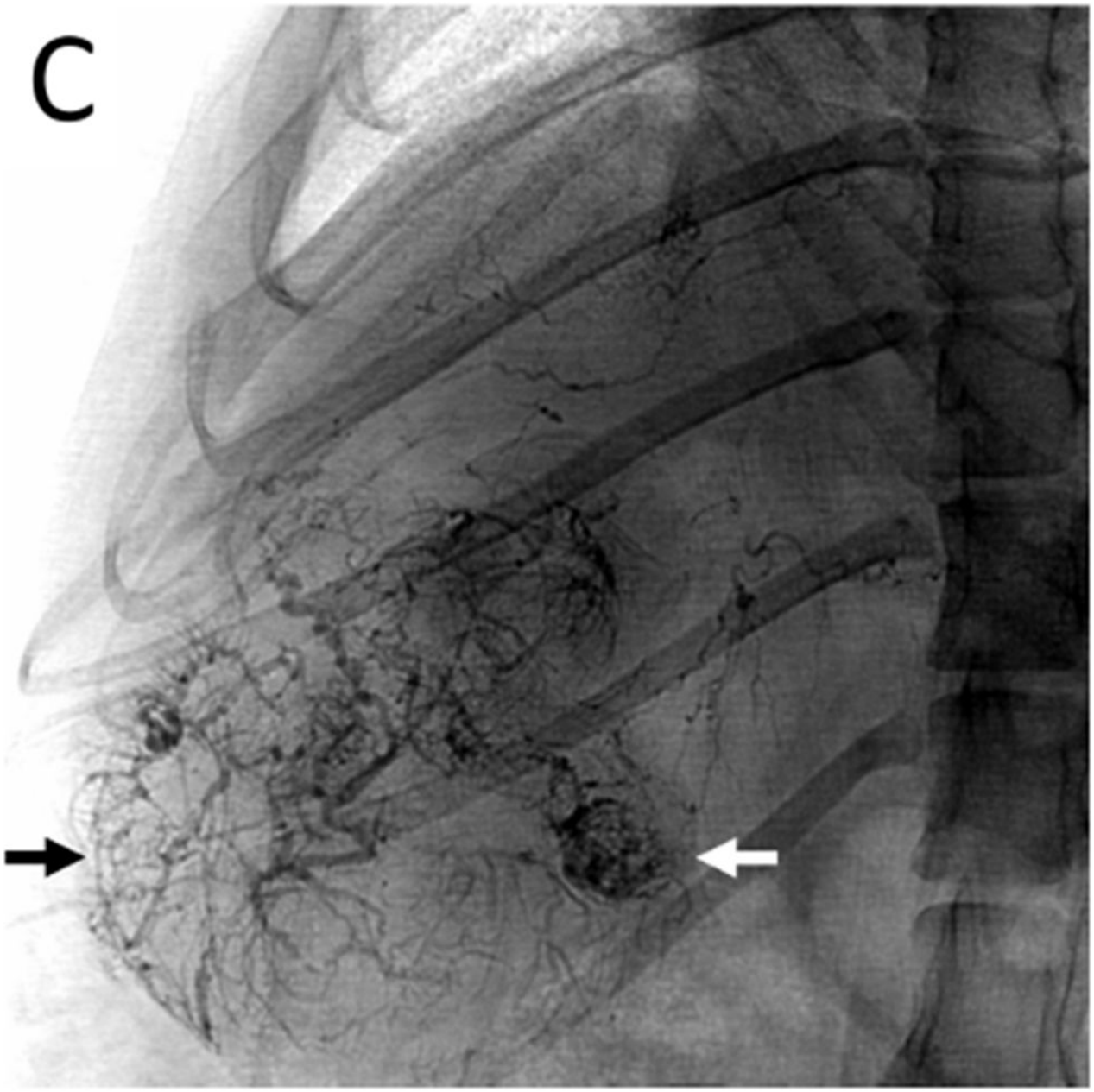

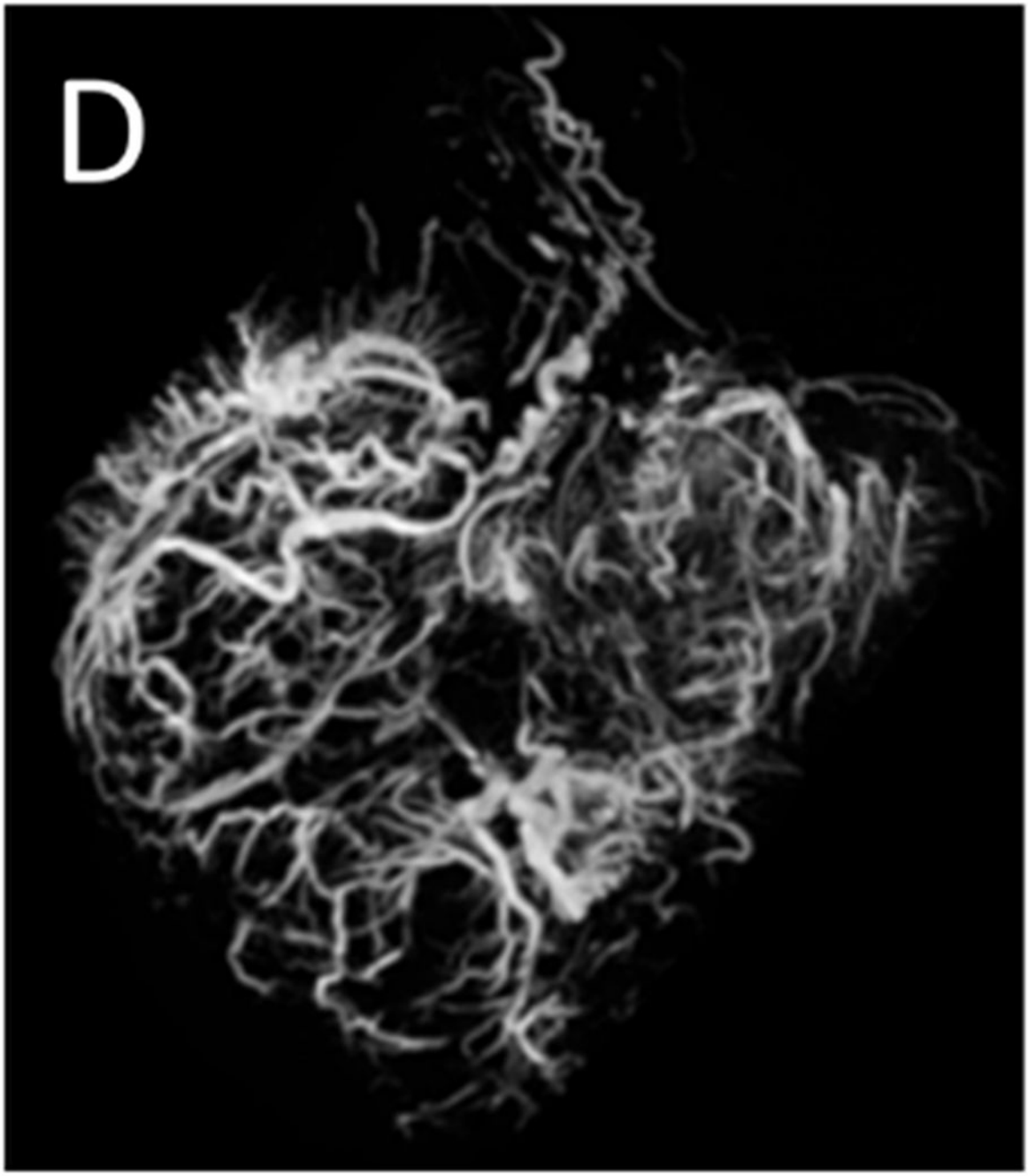

Figure 5.
Post-embolization imaging without contrast administration. Radiopaque drug eluting embolics (arrows) are present within the vasculature of the pedunculated tumor from the same woodchuck shown in Figures 1 and 4. No contrast was administered. (A) Coronal maximum intensity projection image of CBCT; (B) axial MDCT; (C) single fluoroscopic image of the abdomen; and (D) microCT of tumor explant.

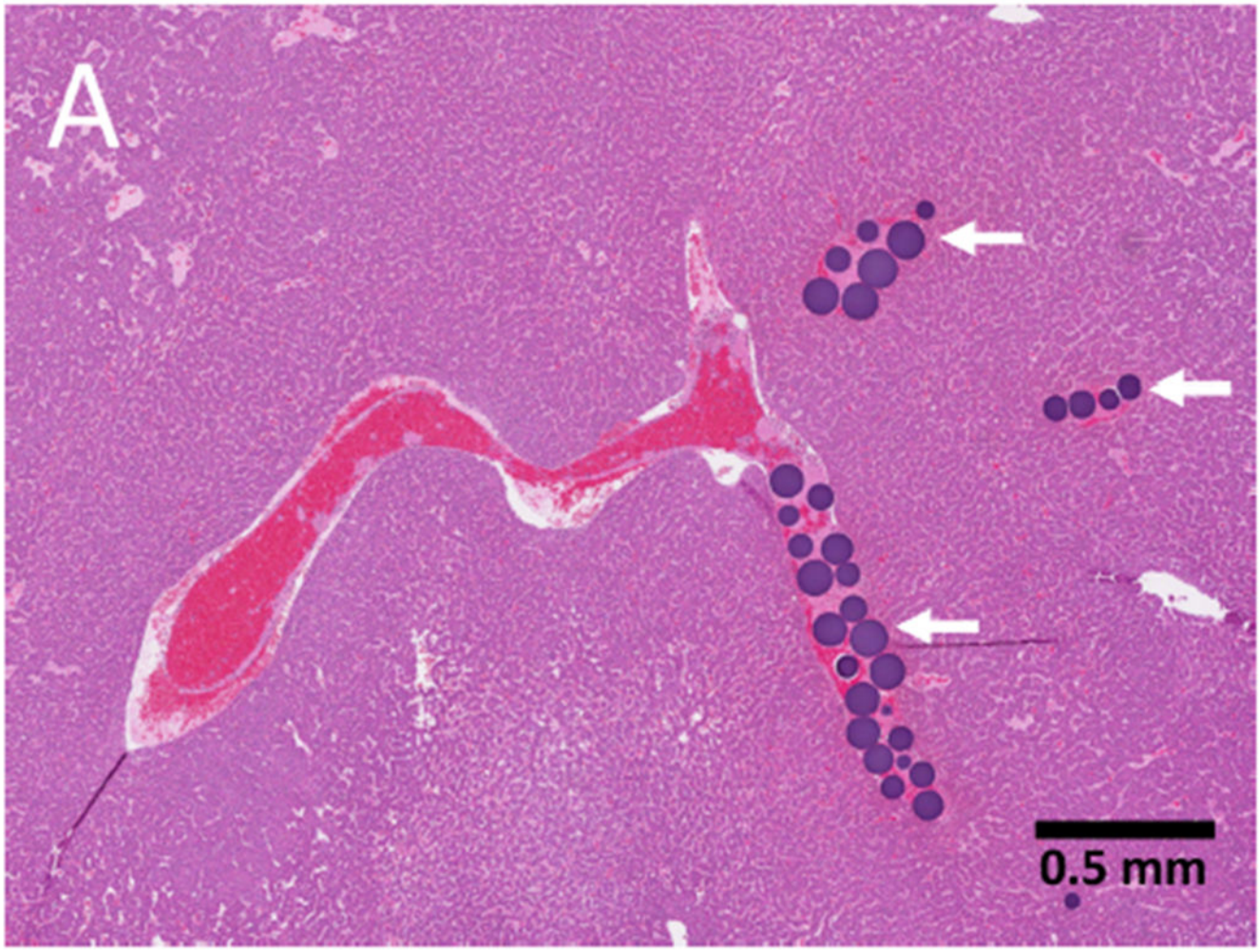

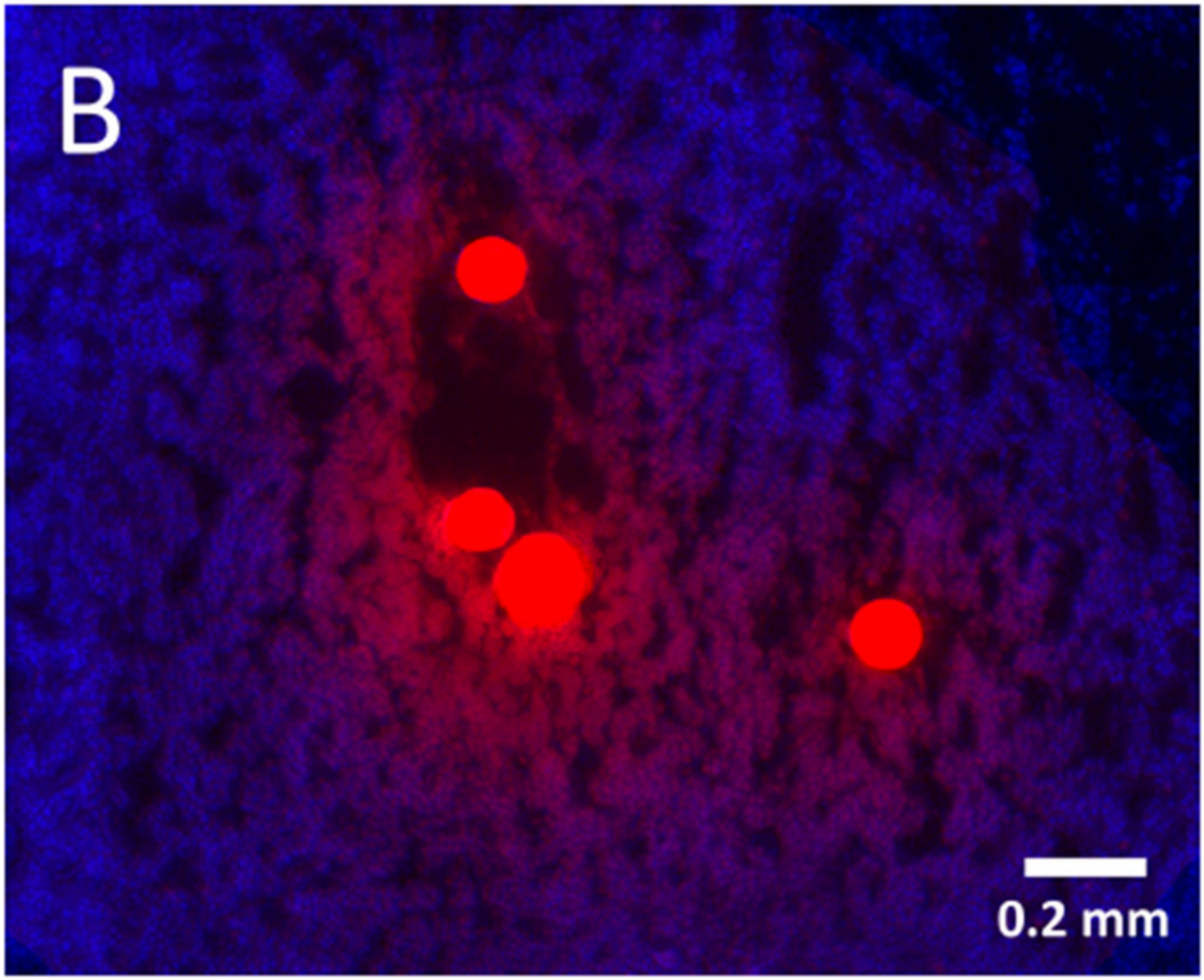

Figure 6.

Hepatocellular carcinoma pathology: drug eluting embolics and drug diffusion into tumor. (A) Histopathology specimen (H&E) of HCC with microspheres (arrows) visible in intratumoral arteries; (B) Fluorescence microscopy of tumor section showing elution of doxorubicin (red) from the microspheres into surrounding tissue (blue, nuclear stain) 45 min post-embolization.